UKAEA FUS 397

UKAEA Fusion
(UKAEA/Euratom Fusion Association)

The HAGIS Self-Consistent Nonlinear Wave-Particle Interaction Models

S D Pinches, L C Appel, J Candy, S E Sharapov,
H L Berk, D Borba, B N Breizman, T C Hender,
K I Hopcraft, G T A Huysmans and W Kerner

March 1998

UKAEA
Fusion

Culham Science Centre, Abingdon
Oxfordshire, OX14 3DB
United Kingdom
Telephone +44 1235 463330
Facsimile +44 1235 463647

The HAGIS Self-Consistent Nonlinear Wave-Particle Interaction Model

S. D. Pinches [a,1,2], L. C. Appel [b], J. Candy [c], S. E. Sharapov [d], H. L. Berk [c], D. Borba [d,3], B. N. Breizman [c], T. C. Hender [b], K. I. Hopcraft [a], G. T. A. Huysmans [d] and W. Kerner. [d]

[a] *Department of Theoretical Mechanics, The University of Nottingham, University Park, Nottingham, NG7 2RD, UK.*

[b] *UKAEA Fusion, D3 Culham Science Centre, Culham, Abingdon, OX14 3DB, UK.*

[c] *Institute for Fusion Studies, The University of Texas at Austin, Austin, Texas, 78712, USA.*

[d] *JET Joint Undertaking, Abingdon, Oxon, OX14 3EA, UK.*

Abstract

The problem of modelling the self-consistent interaction of an energetic particle ensemble with a wave spectrum specific to magnetically confined plasmas in a torus is discussed. Particle motion in a magnetic field coordinate system, whose surfaces are perturbed by a spectrum of finite amplitude magnetohydrodynamical (MHD) waves, is described using a Hamiltonian formulation. Employing the δf method enables the simulation particles to only represent the change in the total particle distribution function and consequently possesses significant computational advantages over standard techniques. Changes to the particle distribution function subsequently affect the wave spectrum through wave-particle interactions. The model is validated using large aspect-ratio asymptotic limits as well as through a comparison with other numerical work. A consideration of the Kinetic Toroidal Alfvén Eigenmode instability driven by fusion born α-particles in a D-T JET plasma illustrates a use of the code and demonstrates nonlinear saturation of the instability, together with the resultant redistribution of particles both in energy and across the plasma cross-section.

Key words: Hamiltonian guiding centre, Lagrangian wave evolution, δf method
PACS: 52.35.-g, 52.65.-y, 52.55.Pi, 52.55.Fa

[1] email: simon.pinches@ipp-garching.mpg.de
[2] Present address: Max-Planck-Institut für Plasmaphysik, EURATOM-Association, D-85748 Garching, Germany.
[3] Permanent address: Associação EURATOM/IST, Av. Rovisto Pais 1096 Lisbon,

1 Introduction

Wave-particle interactions are ubiquitous to physical systems in general and to plasma physics in particular. The distribution of particles in space and energy determines the class of waves able to be supported by the system and in turn, these waves affect the trajectories of the particles, leading to collective and nonlinear evolution of the entire system. This paper describes a means for self-consistently describing an ensemble of energetic charged particles interacting with a spectrum of magnetohydrodynamical (MHD) waves in toroidal plasmas. This work was motivated by an interest in the behaviour of magnetically confined fusion calibre plasmas such as those envisaged by JET and the proposed International Thermonuclear Experimental Reactor (ITER), where the confinement of α-particles is of crucial importance. The methodology may equally be applied to wave-particle interactions in other contexts, such as those occuring in the solar atmosphere for example.

The transport of fusion born 3.52 MeV α-particles across the equilibrium magnetic field is generally negligible on the time-scale for thermalization. However, resonant interaction between a spectrum of Alfvén waves and supra-thermal particles may take place [1,2], leading to significant anomalous transport of the particles. The class of discrete waves considered in this paper are Alfvén eigenmodes (AE) that can exist in the absence of an energetic particle population. Of the various types of AE that have been predicted theoretically, it is the toroidal Alfvén eigenmode (TAE) [3] that is most frequently observed experimentally in toroidal devices. Experiments performed with neutral beam injection (NBI) on tokamaks DIII-D [4], TFTR [5] and with α-particles in D-T plasmas [6] have already shown that weakly damped TAE can indeed be driven by fast particles and that under certain conditions this effect can give rise to significant particle losses [7,8]. Due to the high α-particle pressure in fusion machines such as ITER, it is feared that TAE amplitudes could become sufficiently large for more than 5% of the α-particles to be lost from shot to shot. This level of loss may be sufficient to cause damage to the first wall, whilst larger values could lead to the quenching of ignition [9]. Hence there is a need for studying fast particle interactions with Alfvén eigenmodes in general and with TAE in particular. Note however, that the model presented here is not restricted to Alfvén-like plasma disturbances and may equally well be applied to examine, for example, fishbones or sawteeth [10].

The equilibrium magnetic field structure determines both the orbits of the particles and the spatial structure of the AE that the system can support. A coherent representation of these two facets of the problem requires an appropriate choice of coordinate system. In what follows, the magnetic field structure

---

Portugal.

is represented as a superposition of an axisymmetric equilibrium (which also serves as a coordinate system) obtained from consideration of force balance, to which is added an electromagnetic perturbation representing the TAE. The spatial structure of the perturbation is found from solving the perturbed MHD equations for the particular choice of equilibrium. The perturbations are decomposed into Fourier components in the poloidal and toroidal directions, with each eigenmode allowed two further degrees of freedom: the amplitude and phase-shift, which are undetermined by linear theory. The effect of the fast particles is thus to modify the amplitude and phase of the linear wave — which is expected to retain its radial structure so long as $\beta_{\rm hot}/\beta_{\rm core} \ll 1$. The evolution equations for each eigenmode are derived from a Lagrangian formulation in which wave-particle interactions are included. Nonlinearities arising from wave-wave interactions have been shown to be small [11] when $\gamma/\omega \ll 1$, and are subsequently ignored.

It is apparent that the model presented in this paper [12] is nonlinear, since both waves and particles evolve in response to the collective motion of the other, necessitating a self-consistent treatment. For the problem to be mathematically and computationally tractable requires the imposition of several simplifying, yet plausible assumptions which enable the system to be solved.

Recent developments [13–17] have suggested an enhanced algorithm for performing such simulations that has earned the epithet 'δf method'. This produces less noisy results without the requirement for an excessive number of simulation points through using these points to only model the *change* in the particle distribution function rather than the whole ensemble.

In the early studies of the problem, without the δf formalism, the main results for nonlinear wave-particle resonant interaction were obtained for the 1D bump-on-tail instability [18] and for the TAE with enormous strains upon computing resources. As mentioned above, the δf formalism was found to be the most efficient method for the modelling of wave-particle resonant interactions.

The first successful results for the nonlinear evolution of TAE instabilities were obtained by Fu and Park [11] using 200,000 particles without using the δf technique. In this work the contribution of the energetic particles was taken into account in the form of the pressure-stress tensor. One of the important results of this work was an explicit demonstration that the main saturation mechanism is wave-particle trapping and that wave-wave nonlinearities may be neglected up to wave amplitudes of $\delta B/B \simeq 2 \times 10^{-3}$ at least.

In the mid-1980's White and Chance at Princeton developed a Hamiltonian guiding centre code, ORBIT [19], to examine particle trajectories in the presence of a spectrum of fixed amplitude AE [20]. This code was recently suc-

cessfully used to model the nonlinear interaction of energetic particles and a single AE using a δf approach [21]. However, by choosing to update the wave amplitude from a consideration of energy conservation the treatment of systems with more than one AE becomes impossible. In our code we use a differential equation to continuously update the amplitude and phase of each AE. In particular, this allows us to analyse the behaviour of several AE.

Another advanced approach has recently been used by Berk, Breizman and Pekker [22] to analyse the nonlinear interaction of the resonant particles and an AE using a mapping technique to rapidly describe the particle motion. However, generating the matrix elements for the mapping requires detailed information about both the particle orbits and the wave structure *a-priori*.

In the next section, a brief review of the magnetic field representation is presented for which the equilibrium field lines are straight. Particle drifts in this coordinate system are considerably simplified, but the problem of obtaining the equations of motion and identifying conserved quantities remain. This is facilitated using a Hamiltonian formulation. The interaction of the particles with the spectrum of perturbing MHD waves and the evolution of these waves is described using a Lagrangian approach. In section 3, the δf method is described, and its implementation for isotropic and anisotropic fast particle distributions is elucidated. Section 4 describes the numerical methods used to implement the model and section 5 discusses the various tests that have been performed to validate the code, both in terms of asymptotic limits that obtain for a high magnetic field quasi-cylindrical tokamak and by comparison with numerical results produced by other codes. Section 6 uses the code to simulate a Kinetic TAE interacting with a slowing down distribution of α-particles in a JET tokamak plasma. The final section summarizes the work and discusses the problems that the code is able to tackle.

2 Dynamical Equations

The problem is formulated in a coordinate system determined by the equilibrium magnetic field structure with the ultimate aim being to obtain a simple form for the Hamiltonian description of the particle motion. Assuming that the magnetic field is toroidally symmetric and in scalar pressure equilibrium allows the adoption of the Boozer coordinate system used by White and Chance [19]. This is a straight field line representation which enables the fast streaming of particles along the field lines to be separated from the slow perpendicular drift, combined with the property that the magnetic field components required to describe the particle motion are functions of the flux label alone. The coordinate system takes the poloidal flux ψ as the radial coordinate with the toroidal angle coordinate ζ chosen to obtain straight field lines. The general

poloidal angle θ is prescribed by selecting a specific form for the Jacobian to obtain a covariant representation of the magnetic field in which the field components B_θ and B_ζ are functions of ψ alone. Toroidal symmetry implies that all equilibrium quantities such as the metric tensor and field components are independent of the azimuthal angle ζ. With this choice, $\mathbf{B}$ may be written as

$$\mathbf{B} = \nabla\chi \wedge \nabla\theta + \nabla\zeta \wedge \nabla\psi, \tag{1a}$$
$$= \nabla(\zeta - q\theta) \wedge \nabla\psi, \tag{1b}$$

where χ is the toroidal flux, since the safety factor

$$q(\psi) = \frac{\mathbf{B} \cdot \nabla\zeta}{\mathbf{B} \cdot \nabla\theta} = \frac{d\chi(\psi)}{d\psi}. \tag{2}$$

From (1a), it follows that the vector potential $\mathbf{A}$ can be written as

$$\mathbf{A} = \chi\nabla\theta - \psi\nabla\zeta. \tag{3}$$

The corresponding covariant form of $\mathbf{B}$ is

$$\mathbf{B} = \delta(\psi, \theta)\nabla\psi + I(\psi)\nabla\theta + g(\psi)\nabla\zeta, \tag{4}$$

with the Jacobian written in the form

$$\mathcal{J} \equiv \frac{1}{\nabla\psi \cdot \nabla\theta \wedge \nabla\zeta} = \frac{I + gq}{B^2} \tag{5}$$

to ensure that $B_\theta = \mathcal{J}B^2 - g(\psi)q(\psi) \equiv I(\psi)$.

The dependence of the angular covariant components I and g on ψ alone arises from the choice of Jacobian and is an important ingredient in the development of the Hamiltonian formulation. The radial covariant component δ can be found from $\mathbf{B} \cdot \nabla\psi = 0$ giving

$$\delta(\psi, \theta) = -\frac{I\nabla\theta \cdot \nabla\psi + g\nabla\zeta \cdot \nabla\psi}{|\nabla\psi|^2} = -\frac{I\mathrm{g}^{12} + g\mathrm{g}^{13}}{\mathrm{g}^{11}},$$

where the superscripted terms g^{ij} represent the contravariant components of the metric tensor $\overleftrightarrow{\mathrm{g}}$ and the triplet ordering is (ψ, θ, ζ). As may be seen, δ is related to the degree of non-orthogonality of the system and is very small for equilibria with nearly circular cross-section.

The motion of the background thermal ions is adequately described by a magnetohydrodynamic representation. Energetic ions however, cannot be treated in this way since their drifts due to the curvature and gradient of the magnetic field are comparable with or larger than their electrostatic drifts. Consequently an alternative approach must be developed. The guiding centre Lagrangian is obtained from that for a charged particle in an electromagnetic field through a gyro-averaging procedure [23] which reduces the phase space of the problem. Once canonical variables have been identified, the equations of motion follow by differentiating the guiding centre Hamiltonian with respect to these canonical variables.

Littlejohn [23] showed that the guiding centre Lagrangian L, could be written as

$$L = e\mathbf{A}^{*} \cdot \dot{\mathbf{x}} + \left(\frac{m}{e}\right) \mu \dot{\xi} - \mathcal{H}, \tag{6}$$

where ξ is the gyro-phase, μ is the magnetic moment and $\dot{\mathbf{x}}$ is the guiding centre velocity and represents the total time derivative of the guiding centre location, $\mathbf{x}$. The term $\mathbf{A}^{*} = \mathbf{A} + \rho_{||}\mathbf{B}$ is known as the 'modified vector potential' [24] and is defined through the 'parallel gyroradius' $\rho_{||} = v_{||}/\omega_{ci}$, where $v_{||}$ and ω_{ci} are respectively the parallel velocity and gyro-frequency of the particle. The particle Hamiltonian is given by

$$\mathcal{H} = \frac{1}{2} m v_{||}^{2} + \mu B + e\Phi. \tag{7}$$

where Φ is the scalar potential. The units used are based around characteristic system quantities: the mass and charge of the fast particles, the toroidal major radius at the magnetic axis and the inverse fast particle cyclotron time at the magnetic axis.

Canonical variables are obtained by substituting the expressions for $\mathbf{A}$ and $\mathbf{B}$ given above in equations (3) and (4) into equation (6) and rewriting it as

$$L = \sum_{j} p_j \dot{q}_j - \mathcal{H}. \tag{8}$$

Once this form is obtained, the canonical momenta p_j and coordinates q_j are immediately identified. Including a small electromagnetic perturbation described by the vector and scalar potentials

$$\tilde{\mathbf{A}}(\mathbf{x}, t) = \tilde{A}_{\psi} \nabla\psi + \tilde{A}_{\theta} \nabla\theta + \tilde{A}_{\zeta} \nabla\zeta \quad \text{and} \quad \tilde{\Phi}(\mathbf{x}, t), \tag{9}$$

means that the fast particle Lagrangian becomes,

$$\mathcal{L} = \left(\rho_{\|} I + \chi + \tilde{A}_\theta\right)\dot{\theta} + \left(\rho_{\|} g - \psi + \tilde{A}_\zeta\right)\dot{\zeta} + \mu\dot{\xi} - \mathcal{H} + \left(\delta\rho_{\|} + \tilde{A}_\psi\right)\dot{\psi}. \quad (10)$$

The final term in this Lagrangian may be neglected because the total time derivative $\frac{d}{dt}(\delta\rho_{\|}\psi)$ can be subtracted from $\mathcal{L}$ without altering the equations of motion that are obtained; the terms that remain are higher order in ρ and may be neglected [19,25]. The canonical variables are then readily identified to be

$$P_\theta = \rho_{\|} I + \chi + \tilde{A}_\theta, \quad (11a)$$
$$P_\zeta = \rho_{\|} g - \psi + \tilde{A}_\zeta, \quad (11b)$$
$$P_\xi = \mu. \quad (11c)$$

This leads via the usual Hamiltonian equations of motion to a set of 4 first order differential equations for each of the N_p particles. Obviously, it is impractical to attempt to solve such a system of equations for a realistic distribution of guiding centres, hence one should think of each of these 'particles' as weighted *markers*, with each marker representing a discrete volume of the particle distribution function. In this way the entire fast particle distribution may be represented with a feasible number of differential equations.

The general set of particle guiding centre equations that follows from this formulation are:

$$\dot{\theta} = \frac{1}{D}\left[\rho_{\|} B^2(1 - \rho_{\|} g' - \tilde{A}'_\zeta) + g\left\{(\rho_{\|}^2 B + \mu)B' + \tilde{\Phi}'\right\}\right], \quad (12a)$$

$$\dot{\zeta} = \frac{1}{D}\left[\rho_{\|} B^2(\rho_{\|} I' + q + \tilde{A}'_\theta) - I\left\{(\rho_{\|}^2 B + \mu)B' + \tilde{\Phi}'\right\}\right], \quad (12b)$$

$$\dot{P}_\theta = -\frac{\rho_{\|} B^2}{D}\left[(\rho_{\|} g' - 1 + \tilde{A}'_\zeta)\frac{\partial \tilde{A}_\theta}{\partial\theta} - (\rho_{\|} I' + q + \tilde{A}'_\theta)\frac{\partial \tilde{A}_\zeta}{\partial\theta}\right] - (\rho_{\|}^2 B + \mu)\frac{\partial B}{\partial\theta} - \frac{\partial\tilde{\Phi}}{\partial\theta}, \quad (12c)$$

$$\dot{P}_\zeta = -\frac{\rho_{\|} B^2}{D}\left[(\rho_{\|} g' - 1 + \tilde{A}'_\zeta)\frac{\partial \tilde{A}_\theta}{\partial\zeta} - (\rho_{\|} I' + q + \tilde{A}'_\theta)\frac{\partial \tilde{A}_\zeta}{\partial\zeta}\right] - \frac{\partial\tilde{\Phi}}{\partial\zeta}, \quad (12d)$$

where primes denote differentiation with respect to ψ, steady state electrostatic potential components are neglected (but may be trivially included) and

$$D = \rho_{\|}[gI' - g'I] + I + qg - I\tilde{A}'_\zeta + g\tilde{A}'_\theta.$$

Although these equations completely describe the guiding centre motion they do not represent the easiest numerical scheme to implement since it is necessary to invert the equations for P_θ and P_ζ to obtain ψ and $\rho_{\|}$. A more

practical approach is to evolve ψ and $\rho_{||}$ directly by means of their total time derivatives. $\dot{\psi}$ is simply expressed through the chain rule and equations (11). Once $\dot{\psi}$ is known, a simple expression for $\dot{\rho}_{||}$ can be formed from either of the expressions for the canonical momenta, equations (11a) or (11b).

$$\dot{\psi} = \frac{1}{D}\left[\left(I\frac{\partial \tilde{A}_\zeta}{\partial \theta} - g\frac{\partial \tilde{A}_\theta}{\partial \theta}\right)\dot{\theta} + \left(I\frac{\partial \tilde{A}_\zeta}{\partial \zeta} - g\frac{\partial \tilde{A}_\theta}{\partial \zeta}\right)\dot{\zeta} + g\dot{P}_\theta - I\dot{P}_\zeta\right], \quad (13a)$$

$$\dot{\rho}_{||} = \frac{1}{I}\left[\dot{P}_\theta - \frac{\partial \tilde{A}_\theta}{\partial \theta}\dot{\theta} - \frac{\partial \tilde{A}_\theta}{\partial \zeta}\dot{\zeta} - \frac{\partial \tilde{A}_\theta}{\partial t} - \left(q + \frac{\partial \tilde{A}_\theta}{\partial \psi} + \rho_{||}I'\right)\dot{\psi}\right]. \quad (13b)$$

These equations are then augmented by equations (12) such that the final system of equations to solve is (12a), (12b), (13a) and (13b) for each particle.

Choosing a particular form for the perturbed vector potential $\tilde{\mathbf{A}}$, the equations of motion may be simplified at the expense of generality. The description of low-β shear Alfvén waves permits the assumptions that $\delta B_{||} = 0$ and $E_{||} = 0$. The first of these conditions places a constraint upon $\tilde{A}_\perp$ which can be encompassed by representing the perturbed magnetic field in terms of the variable, $\tilde{\alpha}(\psi, \theta, \zeta, t)$, defined through the relation

$$\tilde{\mathbf{A}} = \tilde{\alpha}(\mathbf{x}, t)\mathbf{B}. \quad (14)$$

The condition that $E_{||} = 0$ provides a relationship between $\tilde{\alpha}$ and the scalar potential $\tilde{\Phi}$:

$$E_{||} = -\nabla_{||}\tilde{\Phi} - \frac{\partial}{\partial t}(\tilde{\alpha}B_0) = 0. \quad (15)$$

Hence only one scalar field is required to describe the field perturbations arising from the AE present. Substituting for the covariant components of $\tilde{\alpha}\mathbf{B}$ into the above equations of motion produces the same expressions as used by White and Chance [19].

The inclusion of non-ideal finite Larmor radius (FLR) effects within the ideal MHD model to treat kinetic TAE (KTAE) leads to a finite parallel electric field in a thin layer around the $q(\psi) \simeq (m+1/2)/n$ surface. Since the energetic particle orbit width is typically much larger than the width of this layer, the majority of the wave-particle power transfer occurs at surfaces away from this region [26] and it is therefore appropriate to retain the assumption that $E_{||} = 0$ everywhere, to compute the wave evolution.

The perturbative effect of the fast particles upon the waves present in the model manifests itself through changes in the waves' amplitudes and phases, whilst the eigenstructure remains invariant. Each wave, characterized by a

distinct toroidal eigenfunction (index k), has therefore just two degrees of freedom, namely a slowly varying real amplitude A_k and phase σ_k. When decomposed into a sum over poloidal Fourier harmonics m, each wave with frequency eigenvalue ω_k can thus be represented in the form

$$\begin{aligned}\tilde{\Phi}_k &= A_k(t)\mathrm{e}^{-i\sigma(t)}\sum_m \tilde{\phi}_{km}(\psi)\mathrm{e}^{i(\mathbf{k}_{mn}\cdot\mathbf{x}-\omega_k t)} \\ &= A_k(t)\mathrm{e}^{-i\sigma(t)}\sum_m \tilde{\phi}_{km}(\psi)\mathrm{e}^{i(n_k\zeta-m\theta-\omega_k t)},\end{aligned}$$

where the wave vector $\mathbf{k}_{mn} = n\nabla\zeta - m\nabla\theta$, and in general the fixed linear eigenfunction $\tilde{\phi}_{km}$ may be a complex quantity containing information regarding the relative phase-shifts between neighbouring harmonics.

The wave evolution, like the particle motion, can be derived by a consideration of the system Lagrangian. The total system Lagrangian may be resolved into four components: the fast particle Lagrangian $\mathcal{L}_{\mathrm{fp}}$ describing the motion of the energetic ions in an equilibrium field; the interaction Lagrangian $\mathcal{L}_{\mathrm{int}}$ describing the effect of the Alfvén waves upon the particle motion; the background, or bulk, plasma contribution to the Alfvén waves $\mathcal{L}_{\mathrm{bulk}}$; the electromagnetic wave Lagrangian $\mathcal{L}_{\mathrm{em}}$ describing the electromagnetic component of the Alfvén waves.

$$\mathcal{L}_{\mathrm{sys}} = \overbrace{\overbrace{\mathcal{L}_{\mathrm{fp}}}^{\text{Particle Lagrangian given in equation (6)}} + \mathcal{L}_{\mathrm{int}}}^{\text{Wave equations}} + \overbrace{\mathcal{L}_{\mathrm{bulk}} + \mathcal{L}_{\mathrm{em}}}^{\text{Wave Lagrangian, } \mathcal{L}_{\mathrm{w}}}$$

In its simplest form, the interaction Lagrangian for an ensemble of N_p particles and a spectrum of waves may be expressed as,

$$\mathcal{L}_{\mathrm{int}} = \sum_{j=1}^{N_p}(\tilde{\mathbf{A}}_j \cdot \mathbf{v}_j - \tilde{\Phi}_j), \tag{16}$$

where the subscript j refers to the fact that the corresponding quantity is to be evaluated at the spatial location of the jth particle, $(\psi_j, \theta_j, \zeta_j)$, and $\tilde{\mathbf{A}}_j$ and $\tilde{\Phi}_j$ represent the sum of all the contributions from each of the waves present at this point.

The wave Lagrangian [22,26] applicable for perturbative changes in the frequency eigenvalue ($\delta\omega_k/\omega_k \ll 1$) is

$$\mathcal{L}_{\rm w} = \sum_{k=1}^{N_w} \frac{E_k}{\omega_k}\left[A_k^2\dot{\sigma}_k\right], \qquad \text{where} \qquad E_k = \frac{1}{2\mu_0}\int_V \frac{\left|\nabla_\perp \tilde{\Phi}_k\right|^2}{v_A^2} d^3x, \tag{17}$$

and v_A is the Alfvén velocity.

Although the evolution equations for A_k and σ_k are easily obtained from equations (16) and (17) the numerical properties of the ensuing equations of motion may be improved through the introduction of the real quantities $\mathcal{X}_k$ and $\mathcal{Y}_k$ to describe the degrees of freedom of the waves, where

$$A_k(t)\mathrm{e}^{-i\sigma_k(t)} = \mathcal{X}_k(t) - i\mathcal{Y}_k(t).$$

The perturbed scalar potential at the jth particle position can hence be written as

$$\tilde{\Phi}_j = \sum_{k=1}^{N_w}\sum_m \left[\mathcal{X}_k(t)C_{jkm} + \mathcal{Y}_k(t)S_{jkm}\right],$$

from which it also follows that

$$\tilde{\alpha}_j = \frac{1}{B_0}\sum_{k=1}^{N_w}\frac{1}{\omega_k}\sum_m k_{\|m}\left[\mathcal{X}_k(t)C_{jkm} + \mathcal{Y}_k(t)S_{jkm}\right],$$

where

$$C_{jkm} \equiv \Re e[\tilde{\phi}_{km}(\psi_j)\mathrm{e}^{i\Theta_{jkm}}],$$
$$S_{jkm} \equiv \Im m[\tilde{\phi}_{km}(\psi_j)\mathrm{e}^{i\Theta_{jkm}}],$$

and

$$\Theta_{jkm} \equiv n_k\zeta_j - m\theta_j - \omega_k t.$$

Returning to the interaction Lagrangian, it is seen that it may now be written as

$$\mathcal{L}_{\rm int} = \sum_{j=1}^{N_p}\sum_{k=1}^{N_w}\frac{1}{\omega_k}\sum_m (k_{\|m}v_{\|j} - \omega_k)\left[\mathcal{X}_k C_{jkm} + \mathcal{Y}_k S_{jkm}\right]. \tag{18}$$

As indicated above, the relevant Lagrangian to vary to obtain the wave evolution equations is $\mathcal{L}_{\rm int} + \mathcal{L}_{\rm w}$, which from equations (17) and (18) becomes

$$\begin{aligned}\mathcal{L} &= \mathcal{L}_{\rm int} + \mathcal{L}_{\rm w} \\ &= \sum_{k=1}^{N_w} \frac{1}{\omega_k} \left\{ \sum_{j=1}^{N_p} \sum_m (k_{\|m} v_{\|j} - \omega_k) \left[\mathcal{X}_k C_{jkm} + \mathcal{Y}_k S_{jkm} \right] + E_k \left[\mathcal{X}_k \dot{\mathcal{Y}}_k - \dot{\mathcal{X}}_k \mathcal{Y}_k \right] \right\}.\end{aligned}$$

Varying with respect to $\mathcal{X}_k$ and $\mathcal{Y}_k$ gives

$$\dot{\mathcal{X}}_k = \frac{1}{2E_k} \sum_{j=1}^{N_p} \sum_m (k_{\|m} v_{\|j} - \omega_k) S_{jkm}, \tag{19a}$$

$$\dot{\mathcal{Y}}_k = -\frac{1}{2E_k} \sum_{j=1}^{N_p} \sum_m (k_{\|m} v_{\|j} - \omega_k) C_{jkm}, \tag{19b}$$

which forms a set of $2 \times N_w$ first order differential equations describing the time evolution of the waves present.

3 δf Formulation

The step from which the δf method [13–17] takes its name is the decomposition of the fast particle distribution function f into two parts, a prescribed component f_0 and the remaining component δf,

$$f = \underbrace{f_0(\Gamma^{(p)})}_{\text{analytic}} + \underbrace{\delta f(\Gamma^{(p)}, t)}_{\text{markers}}$$

where $\Gamma^{(p)}$ represents the physical phase-space comprised of the six components of space and velocity. The key element of the δf method arises from the choice of f_0 to represent the initial distribution of particles so that only the *change* in the distribution function is represented by the markers, or weighted particles. This affords a favourable reduction in numerical noise in the system of the order $|\delta f/f|^2$ [27]. Each marker is imparted an additional attribute, namely the change in the distribution function at that point, with the evolution of this quantity given by the relevant kinetic equation, which in the absence of sources or sinks becomes $\dot{f} = 0$ and can easily be rearranged to give

$$\dot{\delta f}_j = -\dot{f}_0(\Gamma_j^{(p)}), \tag{20}$$

where j is the index identifying each marker. The separation of f into a prescribed component f_0 and a numerically described component δf is formally

valid in all cases and makes no assumptions regarding the fact that the latter be much smaller than the former. However, it is only for the case where $\delta f \ll f_0$ that substantial reductions in simulation noise are expected. The method becomes analogous to the solution of the Vlasov equation using a fluid model on a Lagrangian grid. The value of the distribution function for each marker is evolved according to the method of characteristics. The position of each marker is the tip of each characteristic of the distribution function, that is, the latest position of one of the natural paths for the solution of the equations. The markers are like particles in that they move in space with the same equations of motion. However, rather than representing single particles, they represent evolving values of the distribution function.

The decomposition of the fast particle distribution function leads to the following transformation rule for integral operators:

$$\int f(\Gamma^{(p)},t)\, g(\Gamma^{(p)},t)\, d\Gamma^{(p)} \longleftrightarrow \int f_0(\Gamma^{(p)})\, g(\Gamma^{(p)},t)\, d\Gamma^{(p)} + \sum_{j=1}^{N_p} \delta f_j(t)\, g(\Gamma_j^{(p)}(t),t)\, \Delta\Gamma^{(p)},$$

where $\Delta\Gamma^{(p)}$ is the finite physical phase-space volume element associated with each marker and g is an arbitrary function. If f_0 is specified such that it is toroidally symmetric then upon applying this transformation rule to the continuum form of the wave equations (19) it is found that the term containing f_0 is identically zero, leaving only the contribution from the perturbed part of the distribution function, δf:

$$\dot{\mathcal{X}}_k = \frac{1}{2E_k} \sum_{j=1}^{N_p} \delta f_j \Delta\Gamma_j^{(p)} \sum_m (k_{\|m} v_{\|j} - \omega_k) S_{jkm}, \tag{21a}$$

$$\dot{\mathcal{Y}}_k = -\frac{1}{2E_k} \sum_{j=1}^{N_p} \delta f_j \Delta\Gamma_j^{(p)} \sum_m (k_{\|m} v_{\|j} - \omega_k) C_{jkm}. \tag{21b}$$

As can be seen, the only difference from equations (19) is the inclusion of the additional weighting factor $\delta f_j \Delta\Gamma_j^{(p)} = \delta n_j$, representing the change in the distribution function at each marker location.

Since in the absence of any plasma waves f_0 is expected to be invariant it is defined in terms of the *unperturbed* constants of the motion,

$$f_0 = f_0(P_\zeta^{(0)}, \mathcal{E}^{(0)}; \mu),$$

where $P_\zeta^{(0)} = P_\zeta - \tilde{\alpha} g$, and $\mathcal{E}^{(0)} = \mathcal{E} - \tilde{\Phi}$. This ensures that f_0 does not contribute to the wave growth and allows the statistical noise which would otherwise result from representing f_0 by a finite number of markers to be

reduced. It also ensures that in the absence of any waves the initial number of particles,

$$n_0 = \int_V f_0(P_\zeta^{(0)}, \mathcal{E}^{(0)}; \mu)\, d\Gamma^{(p)},$$

is time-invariant since f_0 has no explicit time dependence. It follows then, that in the absence of any particle sources and sinks the change in the number of particles,

$$\delta n = \int_V \delta f\, d\Gamma^{(p)} = \sum_{j=1}^{N_p} \delta f_j\, \Delta\Gamma_j^{(p)} = 0.$$

The evolution equation for each of the markers that arises from these choices follows from equation (20),

$$\dot{\delta f}_j = -\dot{P}_{\zeta j}^{(0)} \frac{\partial f_0}{\partial P_{\zeta j}^{(0)}} - \dot{\mathcal{E}}_j^{(0)} \frac{\partial f_0}{\partial \mathcal{E}_j^{(0)}}, \tag{22}$$

where it is recalled that within the guiding centre approach μ is an exact invariant and hence does not appear. It is reassuring to note that by specifying $f_0 \equiv 0$ so that $\delta f = f$, then the model regresses to a conventional particle simulation with fixed weight markers, $\dot{\delta f} \equiv 0$.

Equations (21) which describe the wave evolution require the evaluation of $\Delta\Gamma^{(p)}$ at each marker location, this being complicated by the fact that these volume elements are compressible and therefore change with the marker flow. However, their calculation is facilitated by the fact that the flow in canonical space is incompressible (a consequence of Liouville's theorem) and that the canonical volume element associated with each marker $\Delta\Gamma^{(c)}$ is therefore independent of time and need only be calculated once. The relationship between the canonical and physical phase-space elements is described by the Jacobian $\mathcal{J}^{(pc)}(t)$ and provides an elegant way of obtaining the physical phase-space volume elements at any time during the simulation. The caveat, however, is that it is necessary to determine the canonical phase-space volume element associated with each marker.

Uniformly loading some chosen phase-space $\mathcal{U}$ offers a simple solution to the problem of determining the canonical phase-space volume associated with each marker since providing the total phase-volume is known, the volume associated with each marker $\Delta\mathcal{U}$ is trivially calculated. This may then be related to the canonical volume element through the relevant Jacobian, $\mathcal{J}^{(cu)}$. Choosing $\mathcal{U}$ to consist of physically more familiar variables, rather than the canonical

variables, allows the problem to become more intuitive and avoids difficulties associated with inverting the canonical variables into the physical ones. The loading algorithm adopted makes use of an elegant bit reversal scheme described in reference [28].

Employing a δf formulation has not restricted the way in which the physical space of interest is filled with markers. However, assuming that no prior knowledge regarding the regions over which the resonant wave-particle interactions will dominate, it would appear sensible to load markers uniformly throughout the volume. Indeed for the physical case of a fusion population of α-particles interacting with a collection of TAE the resonance structure may become so rich so as to fill most of the region anyway. Even for the relatively benign case of only one TAE, the resonant region will have a width associated with it due to the departure of the fast particles from the field lines, and this alone may be as much as half the minor radius of the machine.

The relationship between the various phase-space elements, $\Delta\Gamma_j^{(p)}$, $\Delta\Gamma_j^{(c)}$ and $\Delta\mathcal{U}_j$ can be summarized as

$$\Delta\Gamma_j^{(p)}(t) \equiv \mathcal{J}_j^{(pc)}(t)\, \underbrace{\mathcal{J}_j^{(cu)}(0)\, \Delta\mathcal{U}_j}_{\Delta\Gamma_j^{(c)}(0)}.$$

The method described above is suitable for use with an arbitrary analytic distribution function f_0, however in special cases where f_0 is highly anisotropic in one of the dimensions allows additional simplifications. The fast particle distribution that arises as a result of neutral beam injection (NBI) can be highly anisotropic with all the injected particles' velocity vectors distributed within a narrow cone around $\lambda = 1$ where the pitch angle $\lambda = v_{\|}/v$. The assumption that the velocity distribution is uni-directional permits one of the velocity dimensions to be integrated out, with the consequence that the phase-spaces required to describe the distribution become 4-D. The volume elements and Jacobians used to represent general and uni-directional velocity distributions are summarized in Table 1 where $s = \sqrt{\psi/\psi_1}$ is a normalized radial coordinate and ψ_1 is the value of ψ at the plasma edge.

The distribution of fast particles is specified through the analytic distribution function f_0, which as indicated above is defined in terms of the unperturbed constants of the motion. In general however, it is more natural to specify the distribution function in terms of a radial flux function and the particle energy. This can be achieved by constructing an expression representing an averaged radial flux value $\langle\psi\rangle$ in terms of the constants of the motion, allowing f_0 to be written as,

$$f_0 = f_0(\langle\psi\rangle, \mathcal{E}^{(0)}; \mu).$$

Quantity	General	Uni-directional
$d\mathcal{U}$	$dv\, d\lambda\, ds\, d\theta\, d\zeta$	$dv_{\|\|}\, ds\, d\theta\, d\zeta$
$d\Gamma^{(c)}$	$2\pi\, d\mu\, d\theta\, dP_\theta\, d\zeta\, dP_\zeta$	$2\pi\, d\theta\, dP_\theta\, d\zeta\, dP_\zeta$
$d\Gamma^{(p)}$	$2\pi\, v^2\, dv\, d\lambda\, \mathcal{J}\, d\psi\, d\theta\, d\zeta$	$2\pi\, v_{\|\|}^2\, dv_{\|\|}\, \mathcal{J}\, d\psi\, d\theta\, d\zeta$
$\mathcal{J}^{(cu)}$	$4\pi\, s\psi_1 D v^2/B^2$	$4\pi\, s\psi_1 D/B$
$\mathcal{J}^{(pc)}$	$\mathcal{J}B^2/D$	$v_{\|\|}^2 \mathcal{J}B/D$

Table 1
Volume elements and Jacobians used to represent general and beam-like ($\lambda \equiv 1$) distributions of fast particles.

Clearly the best choice for $\langle\psi\rangle$ is the time-averaged ψ value but to avoid the computational overhead associated with calculating $\langle\psi\rangle$ for each particle it is more convenient to construct an approximate prescription for it in terms of the constants of the motion. This will necessarily depend upon the orbit topology of the particle under consideration. The definition, $P_\zeta^{(0)} = g\rho_{||} - \psi$, allows the averaged value of $\langle\psi\rangle$ to be written as,

$$\langle\psi\rangle = \left\langle \frac{\sigma g(\psi)}{B(\psi,\theta)} \sqrt{2(\mathcal{E}^{(0)} - \mu B(\psi,\theta))} \right\rangle - P_\zeta^{(0)},$$

where σ is the sign of $v_{||}$. For trapped particles it is sufficient to define $\langle\psi\rangle$ as the values of ψ at the tips of their orbits where $v_{||} = 0$, since this is where the particles spend the majority of their time. To lowest order in an inverse-aspect-ratio expansion the definitions covering all classes of particle may be summarized as,

$$\langle\psi\rangle = \begin{cases} \sqrt{2(\mathcal{E}^{(0)} - \mu)} - P_\zeta^{(0)}, & \text{for } \mathcal{E}^{(0)} > \mu \text{ (Co-passing)} \\ -P_\zeta^{(0)}, & \text{for } \mathcal{E}^{(0)} < \mu \text{ (Trapped)} \\ -\sqrt{2(\mathcal{E}^{(0)} - \mu)} - P_\zeta^{(0)}, & \text{for } \mathcal{E}^{(0)} > \mu \text{ (Counter-passing)} \end{cases}$$

which corresponds to the $\langle\psi\rangle$ surfaces indicated in Fig. 1. A simple form for f_0 exploiting these definitions is to specify f_0 as the product of a radial distribution function $h_1(\langle\psi\rangle)$ and an energy distribution function $h_2(\mathcal{E})$:

$$f_0 = C\, h_1(\langle\psi\rangle)\, h_2(\mathcal{E}), \tag{23}$$

where C is determined by specifying a global parameter such as the volume averaged fast particle beta $\langle\beta_f\rangle$, or the ratio of the number of fast ions to the number of background ions, n_f/n_i. The form used in equation (23) is sufficient to represent the main types of energetic particle distributions typically

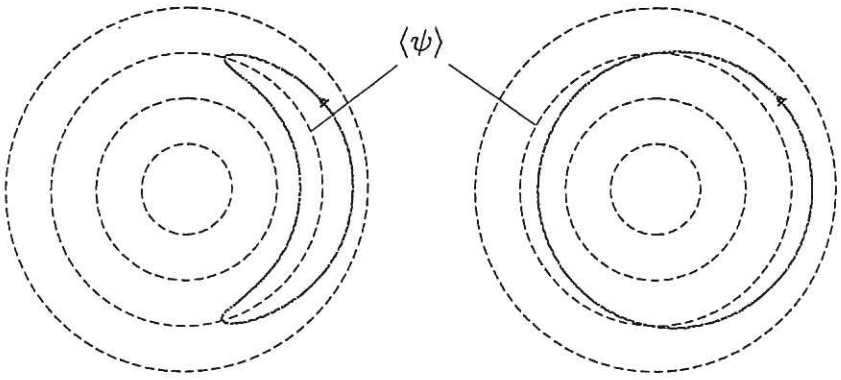

Fig. 1. Characteristic ψ values, $\langle\psi\rangle$, for trapped and passing particles.

found in tokamaks. More general fast particle distribution functions may be represented by modelling (numerical) solutions of the Fokker-Planck equation.

4 Numerical Method

The model developed in the preceding section forms an initial value problem comprised of a system of $5 \times N_p + 2 \times N_w$ first order ordinary differential equations together with appropriate initial conditions. The code written to perform the task of solving them is HAGIS, (**Ha**miltonian **g**uiding centre **i**n **s**ystem.) The HAGIS code is written in standard FORTRAN-77 and has been complied across a variety of platforms. It takes the specified initial conditions together with equations (12a), (12b), (13a), (13b), (21) and (22) to simultaneously advance the spatial location of each marker, its parallel velocity, and the change in the distribution function at that position, as well to update the amplitude and phase of each wave present. The input data required by the HAGIS code consists of three parts; the equilibrium field data, the perturbed field data, and the fast particles' initial conditions. The first of these, the equilibrium data is supplied by the HELENA code [29] by solving the Grad-Shafranov equation and the second by the MHD stability code CASTOR-CR [30,31]. The initial distribution of energetic ions and the initial amplitude and phase of each of the waves are specified in an input data file supplied by the user. An overview of the data handled by the HAGIS code and the other codes which supply it is shown in Fig. 2.

All values and derivatives of the plasma equilibrium required by the code are calculated by splining the equilibrium data. Since the equilibrium is toroidally symmetric this is only necessary over the poloidal plane; 1-D data using radial cubic spline interpolation, and 2-D data using bi-cubic splines with appropriate boundary conditions in the poloidal direction. The HAGIS code uses a 4th order Runge-Kutta integration algorithm chosen in preference to more sophisticated adaptive methods since if the phase-space is properly loaded there is

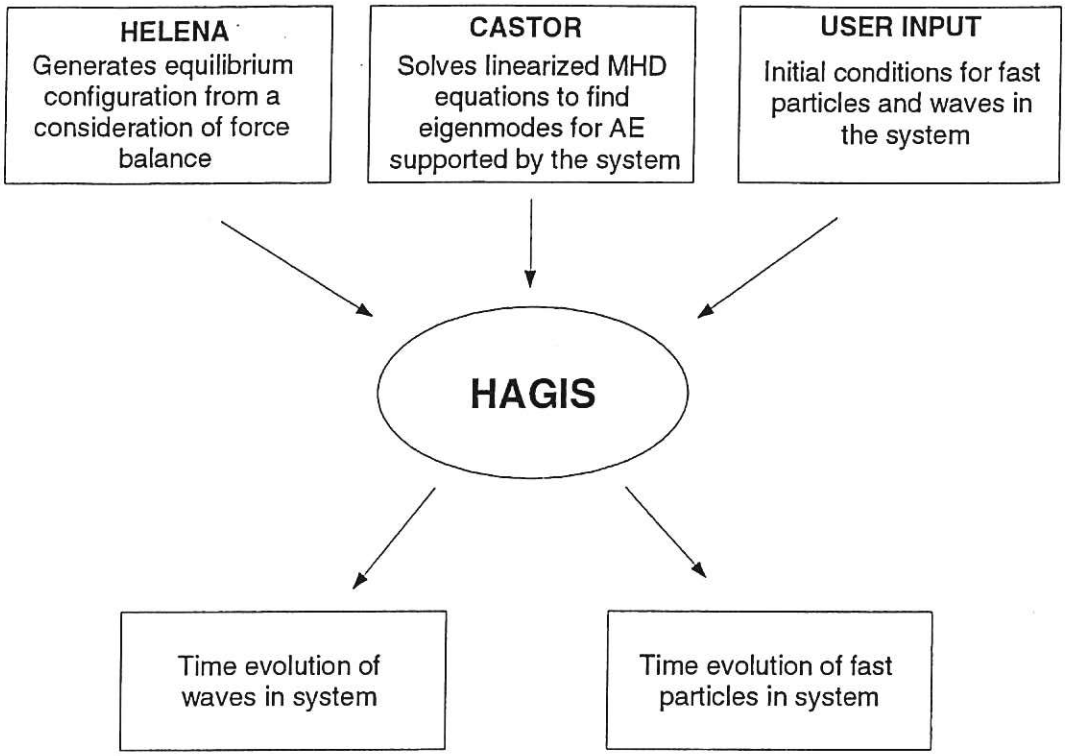

Fig. 2. Overview of the HAGIS code showing flow of data.

no advantage in making modifications to the step size. The accuracy achievable by the model is shown to scale correctly with the integrator step size used and is ultimately limited by the accuracy of the spline representation.

5 Code Validation

To verify the computational implementation of the numerical model and assess its accuracy, the HAGIS code has been extensively tested and validated. In this section the details of some of these tests and comparisons with previous numerical and analytic results are presented.

In the first section the accuracy of the integration algorithm used is assessed by examining the conservation of various system invariants. The examination and comparison of various particle trajectories for which the exact orbits were known, allowing the implementation of equations (12) that describe the particle motion to be verified was described in a previous publication [32]. From a consideration of the behaviour of a single particle in the presence of a fixed amplitude single harmonic wave, it is then possible to test that the correct wave-particle interaction is taking place. The final tests performed were benchmark comparisons with other codes.

The integrator used within the HAGIS model determines the evolution of all the quantities advanced within the model. Consequently a stringent examination of its performance was paramount before any further tests of the code were made. One of the easiest tests to achieve this goal is to examine how well the code conserves various system invariants. In the absence of any field perturbations all the particles can be expected to conserve both energy and toroidal angular momentum since a stationary magnetic field can do no work upon the particles and the equilibria are toroidally symmetric. However, in the presence of a single distinct toroidal eigenfunction,

$$\phi_j = \sum_m \mathrm{e}^{i(n\zeta_j - m\theta_j - \omega t)},$$

particle energy is no longer conserved since $d\mathcal{E}/dt = \partial\mathcal{H}/\partial t \neq 0$. Similarly, ζ_j is no longer a cyclic coordinate and the toroidal component of canonical angular momentum is also not conserved. Thus particle energy and angular momentum can no longer be used as a measure of the code's performance. However using the above ansatz, the field perturbation rotates around the equilibrium field's axis of symmetry and a new constant of the motion exists for each particle,

$$\mathcal{E}_j - (\omega/n)P_{\zeta_j} = \text{constant}.$$

The additional rotation of the field perturbation in the poloidal direction does not give rise to further constants of the motion due to the inhomogeneity of the equilibrium field with respect to the poloidal angle.

Simulations with a single co-passing ($\lambda = 1$) α-particle in the JET equilibrium summarized in Table 2 have been performed in the presence of a single fixed

Parameter	Value
ε	0.334
R_0	3.0 m
B_0	2.87 T
q_0	0.87

Table 2
JET equilibrium parameters used for examination of integrator performance

amplitude ($\delta B/B = 10^{-4}$) $n = 5$ KTAE shown in Fig. 3. The scaling of $\mathcal{E}_j - (\omega/n)P_{\zeta j}$ with the integrator step size used (measured in terms of the number

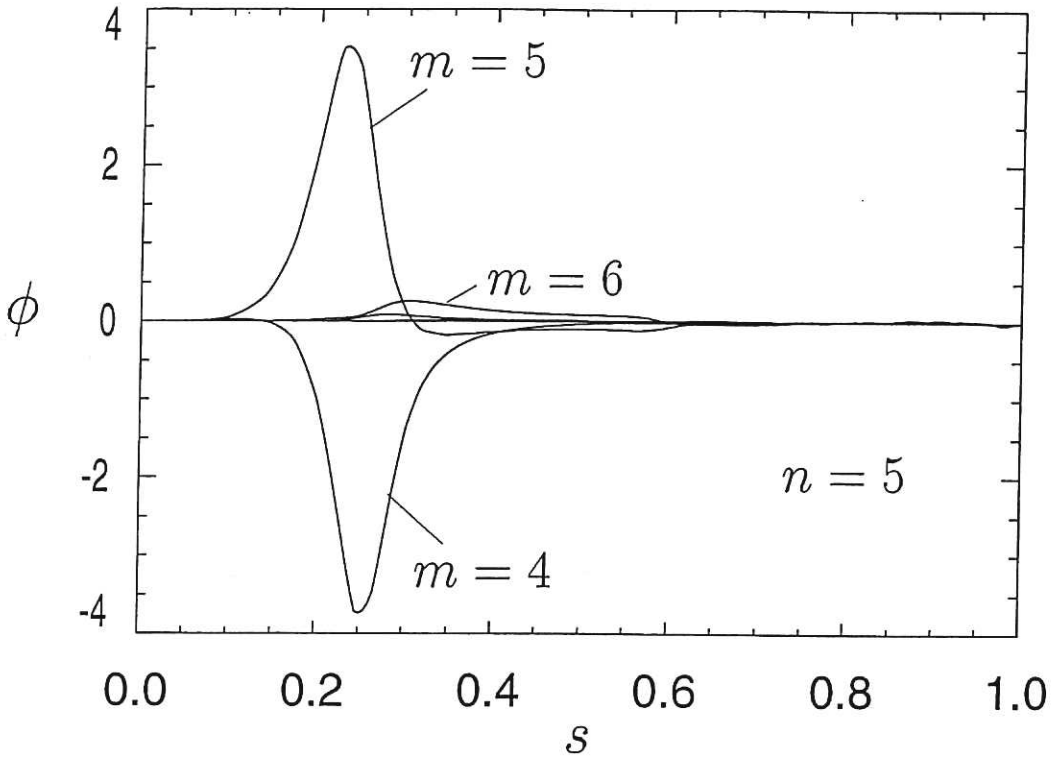

Fig. 3. Principle poloidal harmonics of the $n = 5$ KTAE eigenfunction in JET.

of steps per wave period) is as shown in Fig. 4, showing convergence down to the accuracy of the spline representation which is close to machine precision. The HAGIS code employs a fixed time step 4th order Runge-Kutta integration algorithm and as expected the error scales as approximately $\mathcal{O}(\Delta t^5)$, where Δt is the time step size. The run time of a particular simulation is inversely proportional to Δt. Thus as a compromise between run time and accuracy, Δt is typically chosen such that the integrator makes 64 steps per wave period.

Despite energy and the toroidal component of canonical angular momentum not being conserved for individual particles, the total energy and angular momentum of the wave-particle system is conserved, as it must be for any isolated system. In fact, it can be shown that Fig. 4 may be equivalently viewed as a plot showing the conservation of the total system energy with integrator step size.

5.2 Benchmarking

Due to the complexity of making analytic estimates of quantities associated with the interaction of fast particles with AE, comparisons with other codes are invaluable. They avoid the need to perform simulations within restrictive regimes such as at large aspect ratio ($\varepsilon \ll 1$). For these reasons the HAGIS

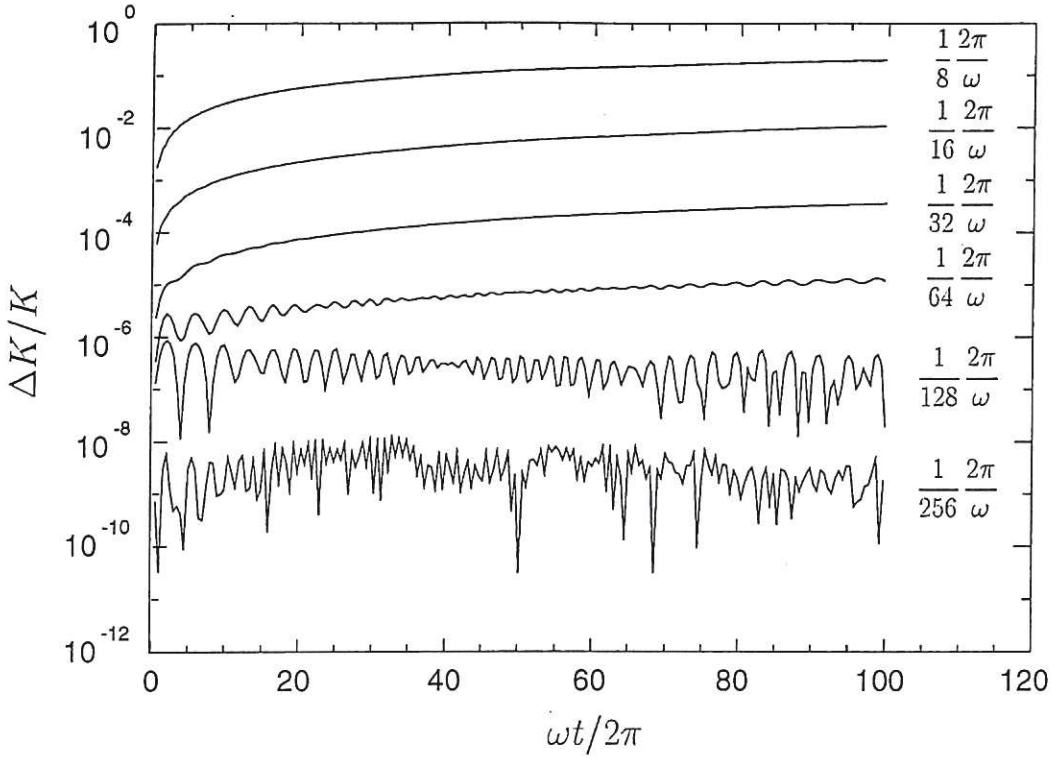

Fig. 4. Plot showing the scaling of the conservation of $\mathcal{E}_j - (\omega/n)P_{\zeta j} = K$ with time measured in terms of the number of wave periods, for various integrator step sizes, Δt.

code has been extensively benchmarked against many other codes including the FAC and CASTOR-K codes.

The FAC code [33] is an independently developed Monte-Carlo δf code employing analytically described equilibria and perturbations to achieve computational performance benefits. The CASTOR-K code [34] is a linearized δW code that uses unperturbed guiding centre orbits. Due to the completely different approach used by this code comparisons with it represent a particularly good test.

5.2.1 Beam-driven TAE

The parameters used for the first comparison are summarized in Table 3 and were chosen such that the simulations fell into the category of small-orbit-width and large-aspect-ratio, allowing additional comparisons with analytical estimates.

The beam distribution used was

$$f_0 = C\,\exp(-2.5\hat{\psi})\exp\left(-\frac{2\mathcal{E}}{\mathcal{E}_0}\right)\delta(\Lambda),$$

Parameter	Value
ε	0.1
R_0	8.011 m
B_0	10 – 50 T
q_0	1.25
n	5
m	7
ω	3.131×10^5 rads/s
f	49.83 kHz
${}^z_n A$	^{4}He
n_i	1×10^{20} m^{-3}
$\langle m_i \rangle$	2.0 m_H
$\langle \beta_f \rangle$	5×10^{-7}
N_p	60000
$\hat{\psi}_j$	(0.02, 0.98)
$\mathcal{E}_j$	(10 keV, 3.8 MeV)
Δt	$2\pi/80\omega$

Table 3
Simulation parameters for beam-driven TAE

where $\Lambda = \mu B_0/\mathcal{E}$, $\mathcal{E}_0 = 3.52$ MeV and the field perturbation used consisted of a single $(m, n) = (7, 5)$ harmonic. The results of scanning in magnetic field intensity are shown in Fig. 5, where the dashed line represents the analytic prediction, whilst the points represent simulations performed using the HAGIS and FAC codes as indicated. The solid line represents results from the CASTOR-K code. The agreement is good, with small differences expected since the CASTOR-K code and the theoretical estimate assumed that the particles had zero orbit width (ZOW) whilst the full orbit width effects were retained within the HAGIS and FAC codes.

For the cases where the phase of the wave was unlocked and allowed to vary self-consistently in time, an additional comparison of the reactive frequency shift with time was possible between that HAGIS and FAC codes. This is presented in Fig. 6 where again good agreement is observed.

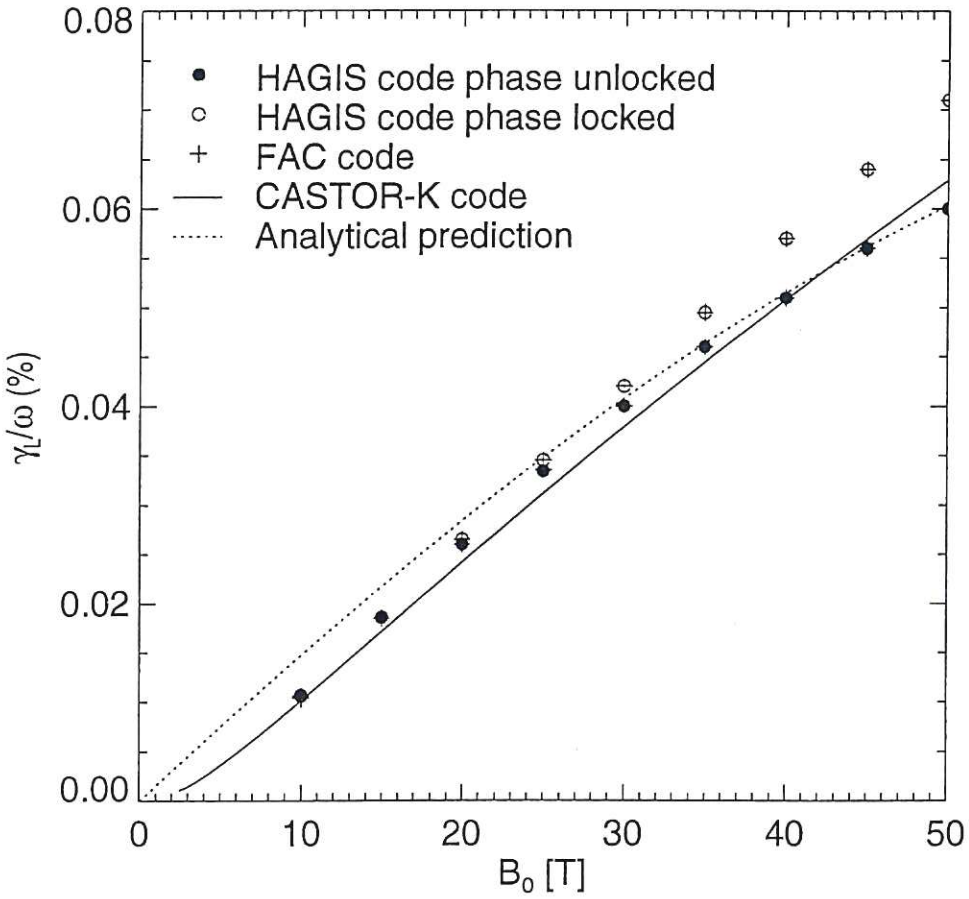

Fig. 5. Variation of linear growth rate with magnetic field intensity.

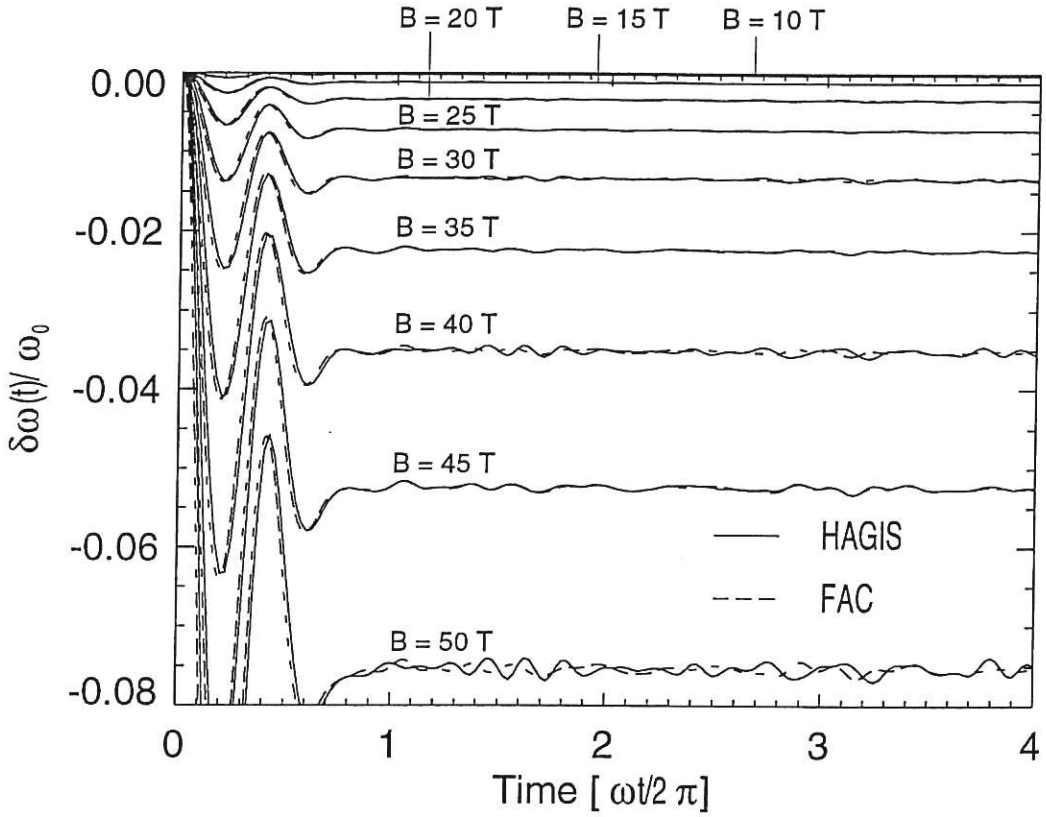

Fig. 6. Comparison of frequency shift for various magnetic field intensities.

5.2.2 *α-particle driven TAE in ITER-like plasma*

The next case compared was that of an isotropic distribution of α-particles in an ITER-like plasma interacting with an AE. The simulation parameters for this test are summarize in Table 4.

Parameter	Value
ε	0.375
R_0	8.0 m
B_0	6.0 T
q_0	0.8375
n	10
m	8, 9
ω	$5.0 \times 10^5 - 8.0 \times 10^5$ rads/s
${}^z_n A$	^{4}He
n_i	1.1×10^{20} m^{-3}
$\langle m_i \rangle$	2.5 m_H
$\langle \beta_f \rangle$	5×10^{-4}
T_e	25 keV
T_i	23 keV
N_p	60000
Δt	$2\pi/80\omega$

Table 4
Simulation parameters for α-driven TAE in ITER-like plasma

The distribution of α-particle used was chosen to represent the expected distribution within an ignited tokamak. The energy distribution of this so-called 'slowing-down' distribution is determined by the effects of electron and ion drag upon the α-particle population. Assuming that the D-T reactants share a common temperature T_i, and that the α-particles are produced with a roughly Gaussian energy distribution, the solution of the Fokker-Planck equation is [17,35],

$$f(\mathcal{E}) = \frac{1}{v^3 + v_c^3} \mathrm{Erfc}\left[\frac{\mathcal{E} - \mathcal{E}_0}{\Delta\mathcal{E}}\right], \tag{24}$$

where the cross over velocity, v_c, is the speed below which the ion drag on the

α-particles becomes dominant and is given by

$$v_c = \left(\frac{3\sqrt{\pi}m_e Z_1}{4m_\alpha}\right)^{\frac{1}{3}} v_{te}, \qquad \text{where} \qquad Z_1 = \sum_i \frac{n_i Z_i^2 m_\alpha}{n_e m_i},$$

v_{te} is the electron thermal velocity and Z_i the charge on the ith species of ion.

The spatial distribution used takes the form of a Fermi distribution function with the parameters chosen to fit those expected in ITER,

$$f(\psi) = \frac{1}{\exp[(\psi - \psi_0)/\Delta\psi] + 1}.$$

ψ_0 is chosen to lie near the $q = 1$ surface since $m = 1$ MHD instabilities (sawteeth) are expected to flatten the distribution within this region [36]. Thus the final distribution used is,

$$f_0 = C \left(\frac{1}{\exp[(\psi - \psi_0)/\Delta\psi] + 1}\right) \frac{1}{\mathcal{E}^{\frac{3}{2}} + \mathcal{E}_c^{\frac{3}{2}}} \mathrm{Erfc}\left[\frac{\mathcal{E} - \mathcal{E}_0}{\Delta\mathcal{E}}\right]$$

with $\psi_0 = 0.2$, $\Delta\psi = 1/14$, $\mathcal{E}_0 = 3.52$ MeV, $\mathcal{E}_c = 329.6$ keV, $\Delta\mathcal{E} = 335.2$ keV.

For this comparison a scan was made in the wave frequency whilst the phase of the wave was held fixed. The results for the three models are presented in Fig. 7 and as can be seen the agreement is again very good. The non-smoothness of the curves is attributed to different classes of particles becoming resonant with different wave frequencies.

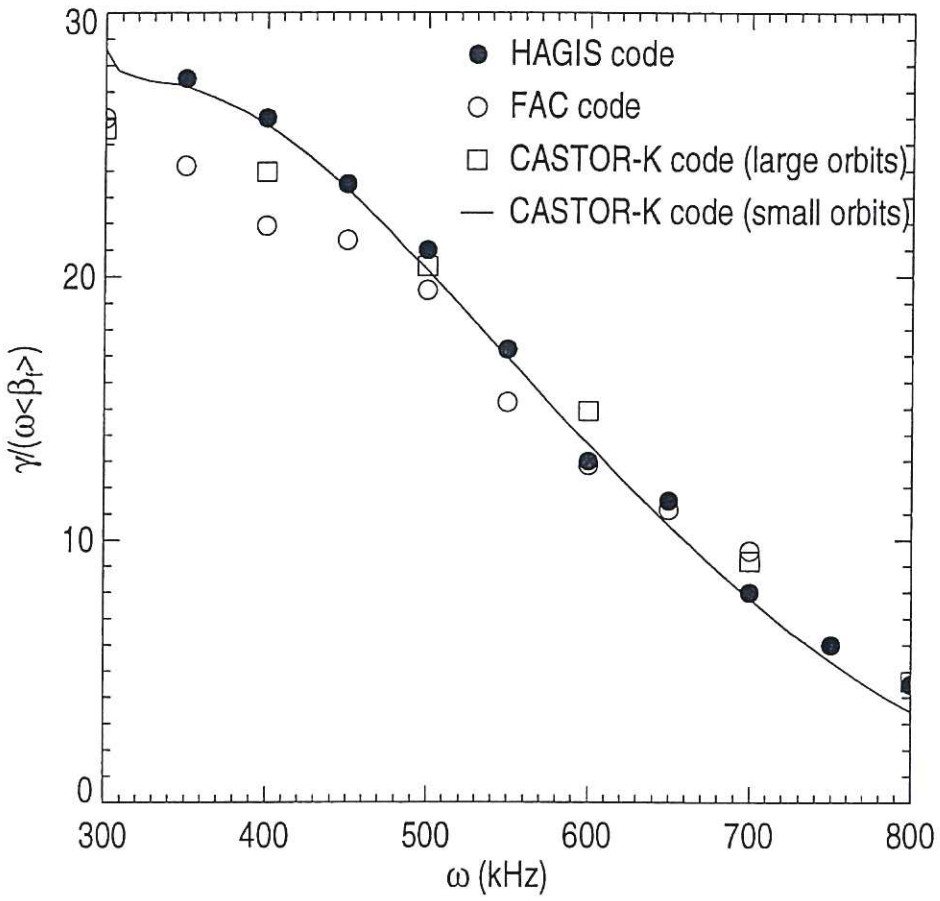

Fig. 7. Comparison of growth rate variation with frequency.

6 Example Application

In this section the HAGIS code is applied to examine the case of a single KTAE interacting with a slowing down distribution of α-particles.

6.1 Resonant Particles

To analyse the structure of the wave-particle resonances, a two dimensional scan has been performed in initial particle energy and launch radius for the case of a JET $n = 5$ AE of amplitude $\delta B/B = 10^{-4}$. The particles considered were deeply passing ($\lambda = 1$) α-particles that were launched up to a maximum energy of $\mathcal{E} = 4.0$ MeV, between $R = 3.1$ m and 3.6 m. Each of the particles were followed for 50 poloidal transits with the change of energy represented in terms of the intensity used in Fig. 8. The complex structure of the reso-

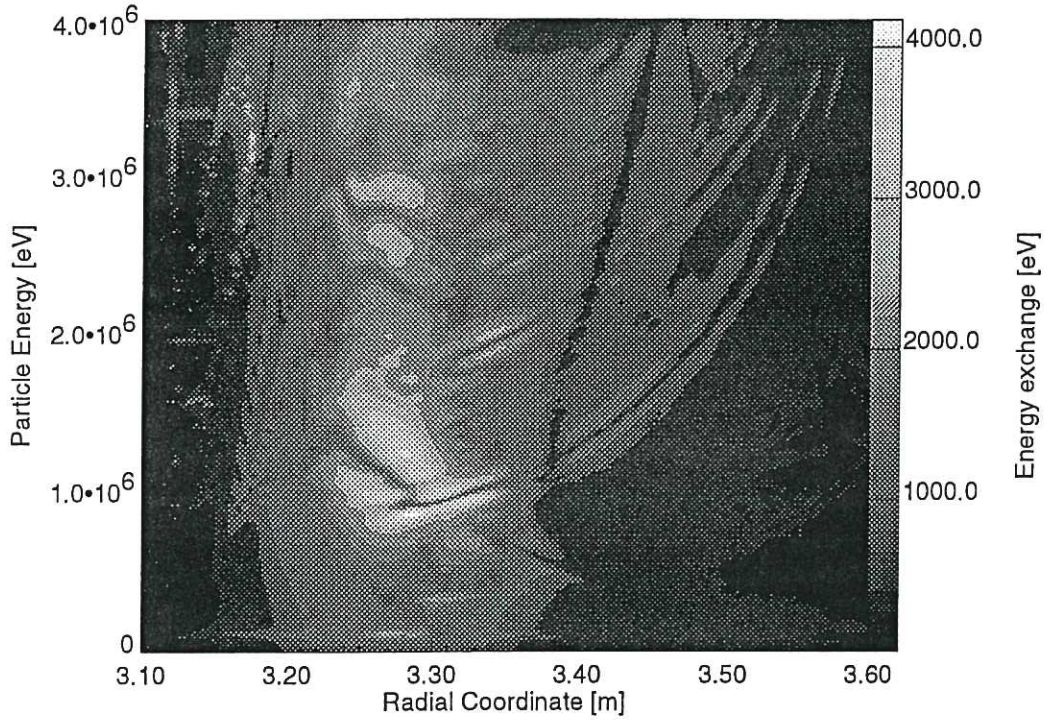

Fig. 8. Wave-particle energy exchange between deeply passing α-particles and an $n = 5$ KTAE. The intensity in the plot represents the amount of wave-particle energy exchanged. The primary resonance corresponding to particles moving at the Alfvén velocity is clearly seen at around 1 MeV and is radially located near the peak in the eigenfunction. The $v_A/3$ sideband resonance is discernable at around 100 keV.

nances (even for deeply passing particles with $\lambda = 1$) necessitates an accurate

representation for the fast particle distribution, especially with respect to energy, since it is seen that there will still be a relatively strong exchange of wave-particle energy near the cut-off energy to which particles are loaded.

Particles that are close to the resonance regions of the phase-space become trapped in the potential well of the AE and the orbits of these particles form island structures. With increasing energy, and therefore increasing orbit deviations from a flux surface, the particles may experience additional side-band perturbations arising from their radial motion across the wave eigenfunction. Particle islands increase in size with AE amplitude and stochasticity arises when these islands, caused by the primary and side-band harmonics, overlap; this process differs from magnetic island stochasticity, in that a single harmonic can give rise to stochastic orbit motions.

6.2 Nonlinear saturation of a KTAE driven by α-particles

In the previous section it was remarked that for wave amplitudes above some threshold particle stochasticity appears in the system. To establish whether this threshold can be achieved due to the free energy source associated with the radial gradient of the α-particles, a self-consistent nonlinear treatment is needed. This section is devoted to the analysis of a KTAE interacting with a distribution of α-particles in JET. Mode damping due to the bulk plasma, particle sources and sinks are not included in this treatment. Hence the case considered is an idealised scenario producing an approximate upper limit for the AE growth rate and saturation amplitude.

The simulations presented in this section address the nonlinear AE evolution by directly simulating the wave evolution and particle re-distribution arising from the interaction of a single $n = 5$ KTAE and the expected distribution of α-particles within a D-T JET plasma. The parameters used for this simulation are summarized in Table 5.

The distribution function was chosen to represent an isotropic slowing down distribution of α-particles,

$$f_0 = C\left(1-\hat{\psi}\right)^3 \frac{1}{\mathcal{E}^{\frac{3}{2}}+\mathcal{E}_c^{\frac{3}{2}}}\mathrm{Erfc}\left[\frac{\mathcal{E}-\mathcal{E}_0}{\Delta\mathcal{E}}\right]$$

where $\mathcal{E}_0 = 3.52$ MeV, $\mathcal{E}_c = 329.6$ keV and $\Delta\mathcal{E} = 335.2$ keV.

The $n = 5$, $m = 4, 5$ eigenfunctions used for these simulations are shown in Fig. 9 along with the q-profile and the radial distribution of fast particles.

Parameter	Value
ε	0.334
R_0	3.0 m
B_0	3.0 T
q_0	0.87
n	5
m	4, 5
f	191.7 kHz
${}^z_n A$	^{4}He
n_i	4.8×10^{19} m^{-3}
$\langle m_i \rangle$	2.5 m_H
$\langle \beta_f \rangle$	5×10^{-3}
N_p	75000
Δt	$2\pi/64\omega$

Table 5
Simulation parameters for α-particle driven $n = 5$ KTAE in JET.

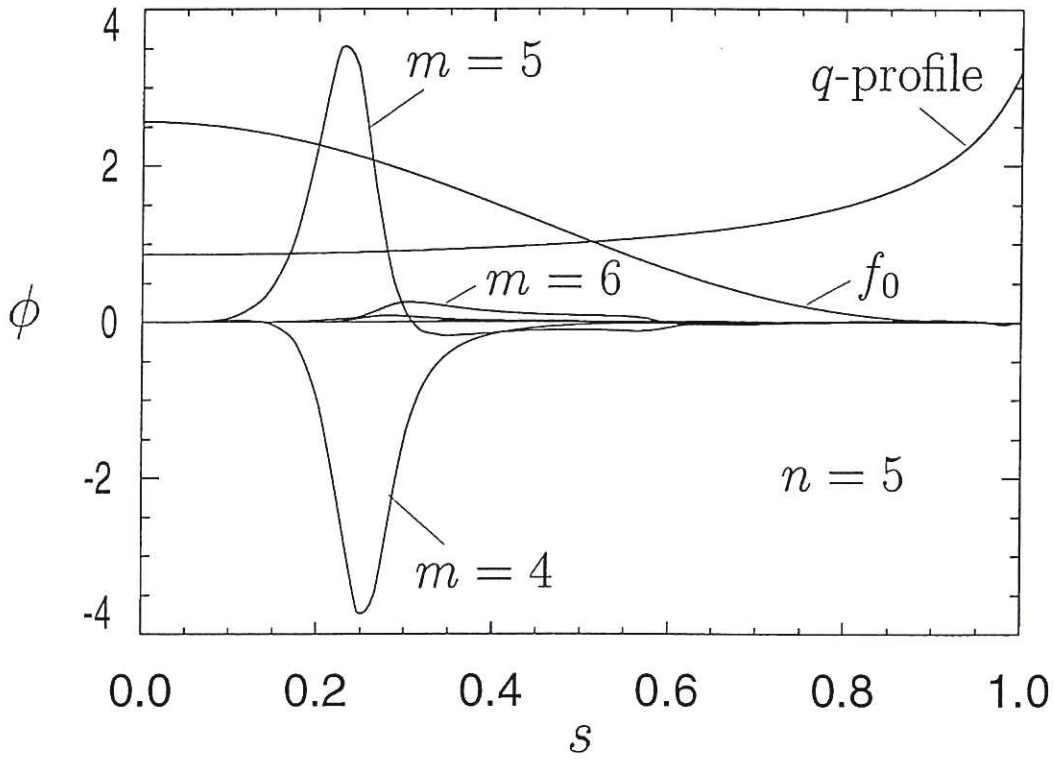

Fig. 9. Plot showing the radial structure of the principle poloidal harmonics of the $n = 5$ KTAE together with the q-profile and the radial distribution of fast particles.

The evolution of the KTAE that resulted from its interaction with this population of α-particles is shown in Fig. 10 depicting the AE amplitude and growth

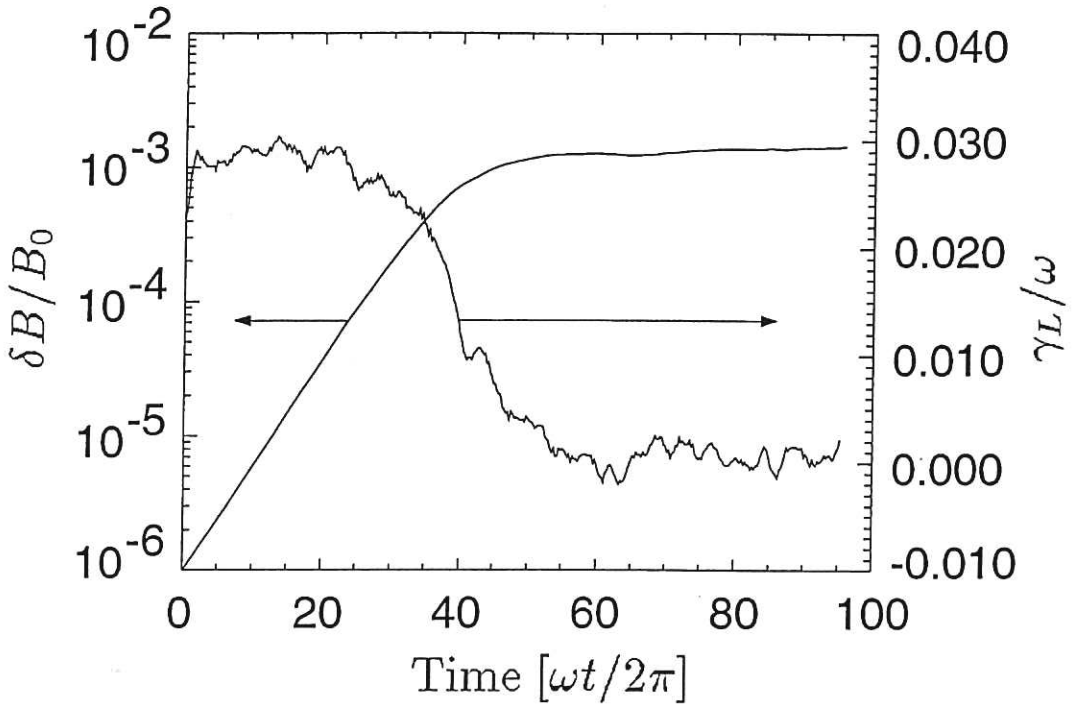

Fig. 10. Evolution of an $n = 5$ KTAE in JET interacting with a slowing down distribution of α-particles.

rate as a function of time. The diagram clearly indicates the two generic stages of the wave evolution that arise in simulations of this type. The first stage is the linear growth stage during which the wave amplitude increases exponentially with time. This behaviour may be understood by observing from equations (21) and (22) that for infinitesimally small δf,

$$\left.\begin{aligned} \dot{A} &\propto \delta f \\ \delta f &\propto A \end{aligned}\right\} \dot{A} \propto A \Rightarrow A = A_0\, \mathrm{e}^{\gamma t}.$$

The second stage in the wave evolution is a saturated state which may be understood by observing that the radial profile of α-particles has been significantly modified such that it no longer acts as a source of free energy, as in Fig. 11. The particle conservation for this simulation is presented in Fig. 12

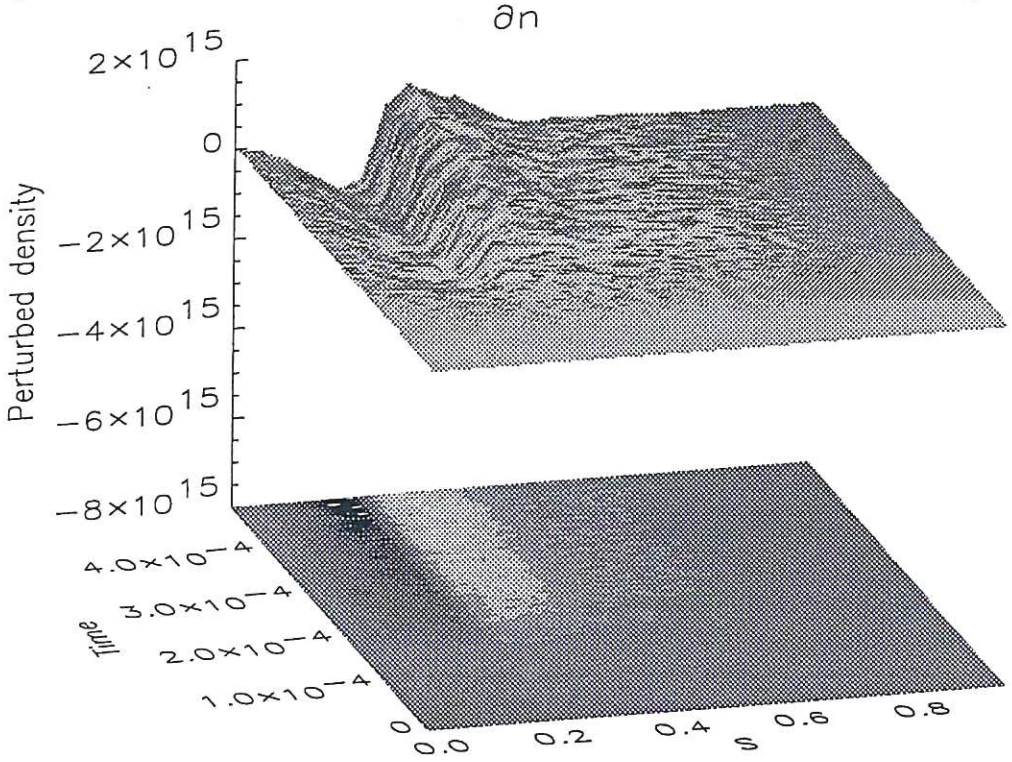

Fig. 11. Radial redistribution of α-particles by $n = 5$ KTAE in JET.

showing the exceptional conservation of particles during the early linear stage and the characteristic oscillatory behaviour following the onset of saturation.

It is interesting to note that the case presented has a growth rate of nearly 3% and saturates by itself at $\delta B/B \sim 10^{-3}$, in quantitative agreement with the results found in [21, see Fig. 11], where an analogous treatment of the wave-particle problem was performed without wave damping, particle sources or sinks.

7 Conclusion

This paper has presented a formulation, implementation and validation of the nonlinear self-consistent δf code HAGIS. This has been developed to investigate the nonlinear resonant interaction of fast particle distributions with linear MHD eigenmodes in toroidal geometry. HAGIS offers a high level of generality: It employs general toroidal solutions of the Grad-Shafranov equation describing tokamak equilibria [29] and a spectrum of linear MHD eigenfunctions of

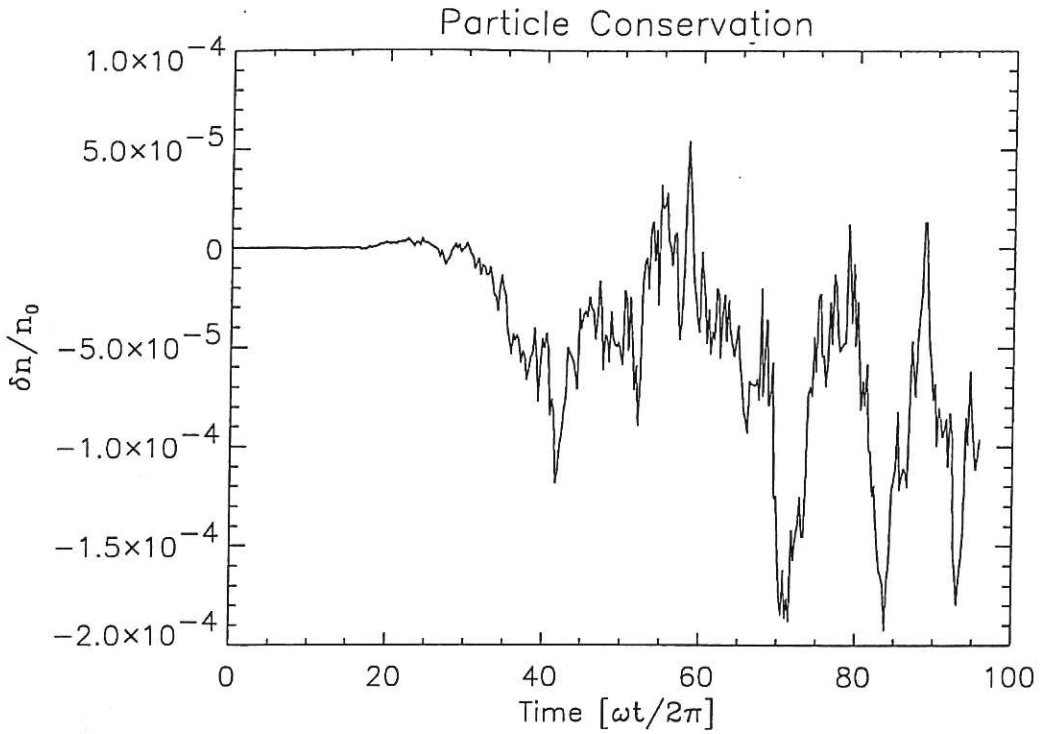

Fig. 12. Conservation of α-particles interacting with $n = 5$ KTAE in JET.

these equilibria generated as solutions of the resistive MHD eigenvalue formulation with FLR corrections [31]. There are no restrictions upon the form of the guiding centre fast particle distribution function.

The code is formulated in Boozer coordinates in which the equilibrium magnetic field lines appear straight upon a flux surface whilst the representation of the magnetic field enables an elegant formulation of the Hamiltonian guiding centre motion. The incorporation of the δf method within the model enables the time dependent solution of the kinetic equation for the deviation from an initially prescribed distribution of fast particles using a finite number of markers whilst still retaining the full orbit effects associated with the field geometry and the nonlinear mode perturbations. Simultaneously and self-consistently the model nonlinearly evolves the spectrum of linear modes present in the system, accurately resolving the linear and nonlinearly-saturated phases of the wave growth and the reactive frequency shifts.

The HAGIS model is applicable for those instabilities for which the principle dynamics of the problem are determined by wave-particle interactions and for which wave-wave nonlinearities may be neglected. The use of the guiding centre approximation restricts the model to phenomena with scale lengths larger than a gyro-radius and slower than the cyclotron frequency. The Lagrangian method of nonlinearly evolving the spectrum of waves present makes the further restriction that the change in amplitude and phase occurs on timescales

much slower than the wave frequency.

The HAGIS code has been validated through comparison with analytical results as well as with other numerical work. For the large aspect ratio, high field, beam-driven TAE case presented, the agreement with both linear theory and other numerical work is very good. For the α-particle driven TAE in an ITER-like plasma the linear growthrates determined using HAGIS compare exceptionally well with other work. Indeed for the simulations shown, the fractional variation of the number of particles represented was $\delta n/n_0 \sim \mathcal{O}(10^{-9})$.

The model has been applied to examine the self-consistent evolution of a single Kinetic TAE and a population of α-particles in a JET plasma, (in the absence of wave damping, or sources and sinks of α-particles). The results presented clearly demonstrate the transition from the linear growth regime into a nonlinearly saturated state with the corresponding self-consistent, anomalous, redistribution of α-particles that arises from the wave-particle interaction. For this case, the resonant regions of phase space for deeply co-passing α-particles and a fixed KTAE amplitude have also been presented. This demonstrates the extensive range of resonances that are present and dispells the notion of being able to consider only 'resonant particles'.

The HAGIS code has many natural areas of applicability beyond the study of Alfvén eigenmode instabilities. For a while it has been known that the sawtooth instability [37] can be suppressed for a limited period of time through particle heating by electromagnetic waves in the ion cyclotron range of frequencies [38,39]. The additional heating creates a strongly anisotropic distribution of trapped energetic particles having positive potential energy that contributes to that of the ideal MHD internal kink mode [40]. Stabilization is achieved because of the reduction in phase space that follows from the conservation of the third adiabatic invariant for minority ions with large bounce-averaged toroidal precessional drift frequencies. HAGIS provides a means for accurately modelling the distribution for such particles in a variety of additional heating senarios. Moreover the potential for sawtooth stabilization by fusion born α-particles is a problem closely allied to this and which is of increasing importance to devices such as ITER, where sawtooth periods of up to 100s have been estimated [41].

Future work with HAGIS will include simulations presenting the effects of sources and sinks of fast particles within the model, as well as the consequences of introducing wave damping. The extension to calculate transport coefficients will also add to making HAGIS an invaluable tool.

Acknowledgement

One of the authors (S.D.P.) gratefully acknowledges financial assistance from UKAEA Government Division Fusion and JET Joint Undertaking during the course of his Ph.D. studies.

The UKAEA authors were jointly funded by the UK Department of Trade and Industry and EURATOM.

References

[1] A. B. Mīkhaĭlovskii, Sov. Phys. JETP **41**, 890 (1975)

[2] M. N. Rosenbluth and P. H. Rutherford, Phys. Rev. Lett. **34**, 1428 (1975)

[3] C. Z. Cheng, Liu Chen and M. S. Chance, Ann. Phys. **161**, 21 (1985)

[4] W. W. Heidbrink et al., Nuclear Fusion **31**, 1635 (1991)

[5] K. L. Wong et al., Phys. Rev. Lett. **66**, 1874 (1991)

[6] R. Nazikian et al, submitted to Phys. Rev. Lett. (1996)

[7] H. H. Duong et al., Nuclear Fusion **33**, 749 (1993)

[8] R. B. White, E. Fredrickson, D. Darrow, M. Zarnstorff, R. Wilson, S. Zweben, K. Hill, Y. Chen and G. Y. Fu, Phys. Plasmas **2**, 2871 (1995)

[9] C. Z. Cheng et al., Proc. 16 IAEA Conf., IAEA/CN/64/FP-23 (1996)

[10] K. McGuire et al., Phys. Rev. Lett. **50**, 891 (1983)

[11] G. Y. Fu and W. Park, Phys. Rev. Lett. **74**, 1594 (1995)

[12] S. D. Pinches, *Nonlinear Interaction of Fast Particles with Alfvén Waves in Tokamaks*, University of Nottingham, (1997)

[13] T.Tajima and F.W.Perkins, Sherwood Theory Meeting, 1983, Paper 2P9 (unpublished)

[14] A. M. Dimits and W. W. Lee, J. Comput. Phys. 107, 309 (1993)

[15] S. E. Parker and W. W. Lee, Phys. Fluids B **5**, 77 (1993)

[16] R. D. Denton and M. Kotschenreuther, J. Comp. Phys 119, 283 (1995)

[17] J. Candy, J. Comp. Phys. **129**, 160 (1996)

[18] H. L. Berk, B. N. Breizman and M. Pekker, Phys. of Plasmas **2**, 8 (1995)

[19] R. B. White and M. S. Chance, Phys. Fluids **27**, 2455 (1984)

[20] D. T. Sigmar, C. T. Hsu, R. B. White and C. Z. Cheng, Phys. Fluids **B4**, 1506 (1992)

[21] Y. Wu, R. B. White, Y. Chen and M. N. Rosenbluth, Phys. Plasmas **2**, 4555 (1995)

[22] H. L. Berk, B. N. Breizman and M. Pekker, in *Physics of High Energy Particles in Toroidal Systems*, American Institute of Physics Conf. Proc. 311, T. Tajima and M. Okamoto, eds (AIP, New York) 18 (1994)

[23] R. G. Littlejohn, J. Plasma Phys. **29**, 111 (1983)

[24] A. I. Morozov and L. S. Solov'ev, *Reviews of Plasma Physics 2*, Consultants Bureau, 1966

[25] R. B. White, Phys. Fluids **B2**, 845 (1990)

[26] B. N. Breizman and S. E. Sharapov, Plasma Phys. Contr. Fusion, **37**, 1057, (1995)

[27] G. Hu and J. A. Krommes, Phys. Plasmas **1**, 863 (1994)

[28] J. H. Halton, Numer. Math. **2** (1960), 84–90 and 196.

[29] G. T. A. Huysmans, J. P. Goedbloed and W. Kerner, Proc. CP90 Conf. Comp. Phys. 1990

[30] W. Kerner, S. Poedts, J. P. Goedbloed, G. T. A. Huysmans, B. Keegan and E. Schwarz, Fusion and Plasma Physics, (1991), 18th Eur. Conf. Berlin, Part IV, p.89

[31] D. Borba, J. Candy, H. Holties, G. Huysmans, W. Kerner and S. Sharapov, in *Proceedings of the 22nd EPS Conference on Controlled Fusion and Plasma Physics*, Bournemouth, U.K. (European Physical Society, Petit Lancy, 1995) Vol. 19C II 237.

[32] L. C. Appel, S. D. Pinches et al., Nucl. Fusion **35**, 1697 (1995)

[33] J. Candy, H. L. Berk, D. N. Borba, G. Huysmans and W. Kerner, Phys. Plasmas 4, 2597 (1997)

[34] D. Borba, J. Candy, W. Kerner and S. E. Sharapov, Proceed. Inter. Workshop on Fusion Theory, Varenna, (1996) (JET Preprint JET-P(96) 35)

[35] J. D. Gaffey, J. Plasma Phys. **16**, 149 (1976)

[36] Proc. Plasma Phys. Workshop on Plasma Theory, Varenna, August 1996

[37] S. von Goeler, W. Stodiek and N. Sauthoff, Phys. Rev. Lett. **33**, 1201 (1974).

[38] D. J. Campbell et al., Phys. Rev. Lett. **60**, 2148 (1988)

[39] C. K. Phillips et al., Phys. Fluids B 4, 2155 (1992)

[40] R. O. Dendy, R. J. Hastie, K. G. McClements and T. J. Martin, Phys. Plasmas **2**, 1623 (1995)

[41] F. Porcelli, D. Boucher and M. N. Rosenbluth, Plasma Phys. Contr. Fusion **38**, 2163 (1996)